Validation of Printed, Skin-Mounted Multi-Lead Electrode for ECG Measurements

Tiina Vuorinen*, Kai Noponen, Antti Vehkaoja, Timo Onnia, Eeva Laakso, Susanna Leppänen, Kirsi Mansikkamäki, Tapio Seppänen & Matti Mäntysalo

M.Sc. T. Vuorinen, M.Sc. K. Noponen, Prof. A. Vehkaoja, B.Sc. T. Onnia, B.HC. E. Laakso, B.HC. S. Leppänen, D.Sc. K. Mansikkamäki, Prof. T. Seppänen & Prof. M. Mäntysalo

M.Sc. T. Vuorinen, B.Sc. T. Onnia, Prof. M. Mäntysalo
Faculty of Information Technology and Communication Sciences, Tampere University, Tampere, Finland
E-mail: tiina.vuorinen@tuni.fi

Prof. A. Vehkaoja
Faculty of Medicine and Health Technology, Tampere University, Tampere, Finland

M.Sc. K. Noponen, Prof. T. Seppänen
Center for Machine Vision and Signal Analysis, University of Oulu, Oulu, Finland

B.HC. E. Laakso, B.HC. S. Leppänen, D.Sc. K. Mansikkamäki
Biomedical Laboratory Science, Tampere University of Applied Sciences, Tampere, Finland

An electrocardiography (ECG) monitoring can be used to detect heart related abnormalities by recording cardiac activity over a period of time. The conventional 12-lead ECG measurement system is the standard practice to evaluate heart's electrical activity. However, the recent trend is to develop patch-type measurement devices for unobtrusive ECG monitoring by reducing device size and number of electrodes on the skin. This development aims to minimize the discomfort for the user by the wearable recording devices.

In this study, we are proposing a printed, bandage type hybrid system for continuous ECG monitoring to make the measurement as comfortable as possible but still maintaining the signal quality required for medical evaluation. Movement artifacts in recorded ECG signal are

a challenge in long term monitoring while the patients are engaged in their everyday activities. In this study, we have compared the movement artifacts between our printed skin-conformable electrode and commercial exercise stress test ECG electrodes during different physical activities and stationary periods. The results show that the signal quality obtained with the multi-lead patch ECG electrode, manufactured with printing technologies, is comparable to electrodes currently used in healthcare.

1. Introduction

World Health Organization (WHO) estimates that 17.9 million persons died as a result of cardiovascular diseases in 2016 (31% of all global deaths).[1] New healthcare solutions are needed to intervene this global issue. Wearable devices and telehealth are enabling a formation of a new segment among healthcare technologies. These medical devices could provide continuous monitoring of risk patients, early symptom detection and reduced healthcare costs. [2] Continuous monitoring is required especially in cardiac healthcare because the cardiovascular disease symptoms may occur at any time of the day. For that reason, different monitoring systems have been developed to detect the cardiac events, and the occurred symptoms define the right monitoring type. Ambulatory electrocardiographic (Holter) monitoring is one option and it is the clinical standard of care for detecting cardiac events. A Holter monitor is a portable measurement device with wire-connected electrodes. Electrodes are attached to the patient's skin to record the low-level electrical potentials originating from the de- and repolarization of the cardiac muscle, during every heartbeat, and are transferred to the body surface by the volume conductor formed by the body tissues. This type of monitoring systems can provide useful information about the function of the heart from diagnostic and prognostic point of view. Nevertheless, they lack the comfort important

for people who would benefit from wearing the monitoring devices for extended periods of time.[3,4]

Due to this, the transition from bulky, wire connected devices to wearable patch type devices is a fast-developing research field.[5–7] This enables the development of totally new types of structures, called epidermal electronics. Epidermal electronics refers to stretchable electronic systems in which the mechanical properties of the device align with the human skin, and the whole system is so light weight and thin that it integrates seamlessly with the epidermis. [8] Due to these properties stretchable electronic systems overcome the mechanical mismatch and are therefore more comfortable to use even for prolonged device wearing time. [4,9,10] Epidermal electronics provides novel structures for imperceptible measurements of skin movements and different biological signals such as temperature, skin hydration and microvascular blood flow, electromyography (EMG) and biochemical and cardiac signals. [4,11–17]

Several types of epidermal electronic systems have been developed to record ECG signals. Lee et al. have developed an ECG and heart rate logging wearable sensor referred as "WiSP". The device is low cost, light-weight (1.2g and 58 mm x 25mm x 1mm) and capable of energy harvesting and capturing one ECG lead at a time (lead I, II, or III).[10] Nawrocki et al. fabricated and tested an ultrathin (sub-300 nm) biopotential electrodes claiming them to be low-noise and motion artifactless. The electrodes were tested by wearing them on the arm and by vibrating the skin with an electromechanical vibrator. [18] Dong et al. presented a stretchable bio-potential electrode for long-term ECG signal recordings and the device was tested with one male volunteer. [19] Temperature sensor together with gel-less sticky ECG

sensor was developed by Yamamoto et al. The ECG sensor was tested with one volunteer so that the sensor patch was attached to the volunteer's chest and the patch was wire-connected to measuring devices. [20]

Long-term wearability, stretchability of mechanically different materials, permeability, and physiological differences between users are critical challenges that need to be overcome before epidermal electronics can be used in real-life applications.[10,18,21,22] For example to minimize the skin irritation of the gel electrodes a lot of research is done to develop gel-free dry electrodes. [23–27] Several studies present new stretchable electrode, sensor and measurement system designs. Nevertheless, these studies lack the comprehensive tests, with both males and females, were the sensors and the processing unit are placed in the exact place where the measurement would be done in real life situations. While in most of the earlier studies the developed patch electrodes are made for single-lead ECG measurement and aimed for monitoring cardiac rhythm, more measurement leads observing the heart from several directions are needed. Multiple leads enable more comprehensive view about the cardiac activity and for example monitoring the level of ST-segment in the ECG and detecting ischemic events.

In this study we compared a printed, multi-lead ECG electrode with Ambu Blue Sensor R-00-S electrodes during different physical activities to estimate differences in their vulnerability to motion artefacts. We recruited volunteers with different body types to verify the functioning in variety of people. The subjects performed two identical approximately 30 minutes long tests with a resting period in between them. Both test rounds were done by wearing either printed ECG electrodes or traditional electrodes. Faros 360 (Bittium Biosignals) recording

device was used to record the signals in both cases. Volunteers were both males and females, with different level of physical performance, from age 23 to 50. We have validated the signal quality obtained with printed multi-lead patch ECG electrode and showed that signal quality, comparable to electrodes currently used in healthcare, can be achieved with compact unobtrusive electrode structure. The long term wearability (72 hours) of the multi-lead patch is presented in [28].

2. Results and Discussion

Figure 1. a) presents the structure and the layers of the developed bandage. Layer one is 50-µm-thick thermoplastic polymer film. Layer two is the same material with screen-printed stretchable silver conductors. Layer three is polyurethane film with an acrylic adhesive layer. Cut-out-holes are made to the layer three and layers 1-3 are then heat-laminated together. Finally, round-shaped pieces of hydrogel were attached to the structure to improve the electrical contact with the skin. Figure 1. b) shows the how the bandage is cut to its final shape by removing excess adhesive material around the print. More detailed description of the bandage structure is presented in the Experimental Section.
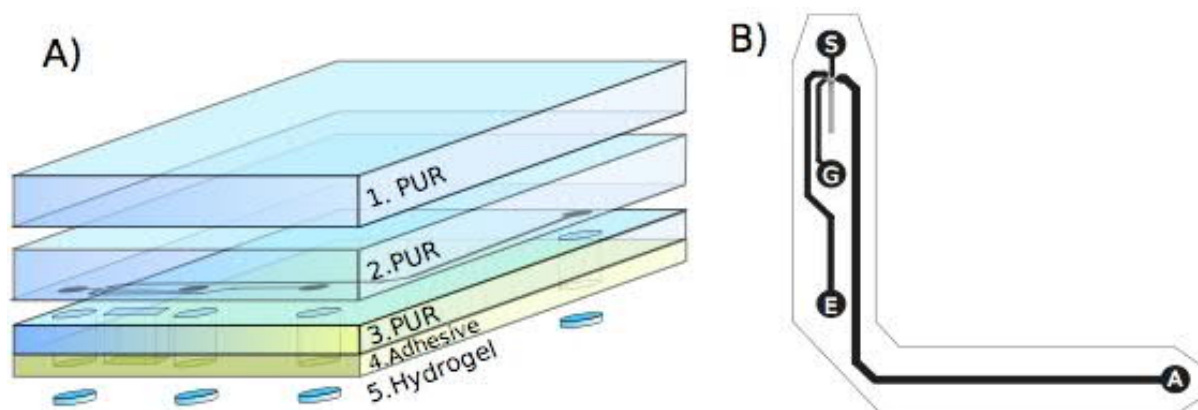
Figure 1. *A) Multilayer bandage structure. The layer 1 is 50 µm-thick thermoplastic polyurethane (TPU) film, the layer 2 is 50 µm-thick polyurethane (TPU) with screen printed*

silver conductors, the layer 3 is polyurethane film and the 4th is an acrylic adhesive. Number 5 are hydrogel pieces. B) illustration of the final bandage layout when it is cut out from the larger area substrate.

To analyze similarities and differences of the signals recorded with traditional electrodes and the proposed bandage, a signal quality comparison study was conducted with 29 volunteers (14 females, 15 males) with no diagnosed cardiac problems. In four cases, the subject's data had to be rejected posteriori due to occurrence of technical problems in the recording leaving a totality of 50 data records, 25 with each electrode type. The most likely cause for the problems was considered to be related to connectivity between the electrode connector and the cabling to the recording device. Participants' characteristics such as age, weight, height, and body mass index are listed in **Table 1**.

Table 1. *Partisipants' characteristics*

	Age (years)	Weight (kg)	Height (cm)	Body mass index
Mean SD	32.2 ±7.6	70.2±9.5	171.3±9.9	24.0±3.0
Range	23-50	54-93	153-195	19.3 - 30.0

As concurrent measurements with the bandage and electrodes from the same electrode locations are not possible, two consecutive incremental exercise tests were made with each subject in a randomized order: one with the bandage and another one with regular electrodes placed at the bandage electrode sites. The measurement protocol included lying still (supine position), standing still, walking/running on a treadmill at increasing speeds, and finally recovering in sitting position. Between the measurements, there was a rest period of one hour. Although the recordings were not made simultaneously, we can draw conclusions on differences in the average behavior and amounts of variation exhibited in the data at similar heart rate levels.

Figure 2 shows the electrode locations in EAS electrode system based on which the evaluated electrode was developed. [29] The electrode E is located on the lower part of the sternum, A on the standard V5 electrode location of the 12-lead system, and S on the manubrium. The electrode potentials are measured with respect to common reference electrode G and three bipolar leads are formed as potential differences between the electrode sites A, E, and S. Namely, the lead AE is the voltage $u_{AE} = \phi_A - \phi_E$, AS is $u_{AS} = \phi_A - \phi_S$, and ES is $u_{ES} = \phi_E - \phi_S$, where ϕ_X denotes the electrical potential at the site X. It should be noted that there are only two independent leads in this set, and e.g. the lead ES is linearly dependent on the two other leads $u_{ES} = u_{AS} - u_{AE}$. Figure 2 b) presents the monitoring system and the printed electrodes secured in place for the measurements.
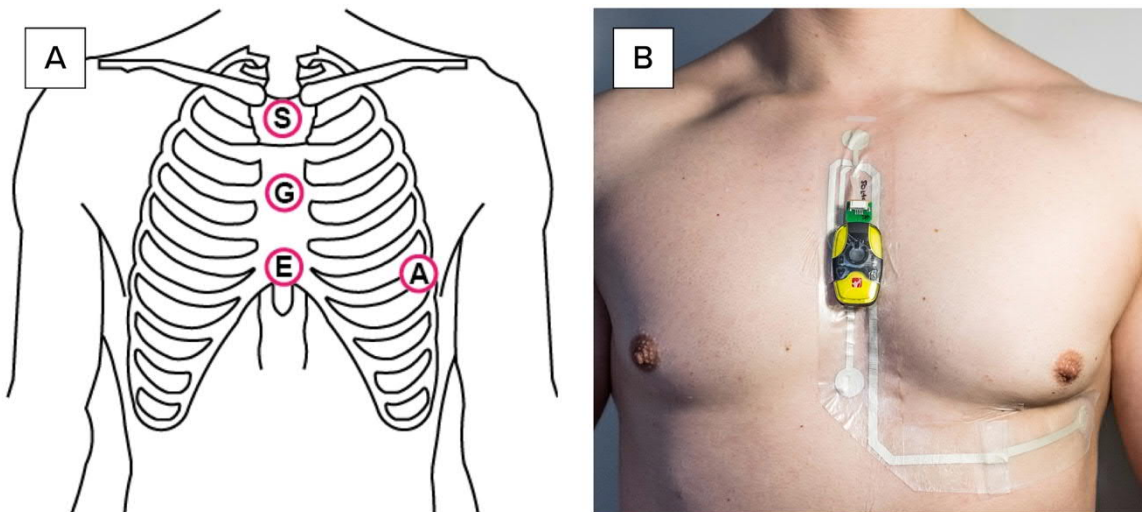

Figure 2. *a) electrode locations in EAS electrode system and b) a picture of a volunteer wearing the bandage and the data collecting device.*

Figure 3 depicts the beat-to-beat variation of the ECG of one randomly selected subject in the AS lead of the EAS electrode configuration. The beat-to-beat variation in the AE, and ES

leads are shown in **Figure S 2** and **Figure S 3** in supporting information. Superimposed heart beat cycles with the characteristic P-waves, QRS-complexes, and T-waves following each other are observed in Figure 3. The signals measured with the bandage are shown on the left, and those with the regular electrodes on the right. From top to down, the signals have been further grouped together according to the exercise test protocol phases of lying still (supine position), standing, walking, brisk walking, and running that represent the increasing work load portion of the test. In each phase, heart rate between the two measurements are similar, and the heart rate does not vary very much within a phase leading to rather stable superimposition. Due to the more varied heart rate range, however, the recovery phase (sitting) of the exercise test is not depicted. Regarding the variation seen in the figures, some changes of the QT-intervals can be seen caused by the changing heart rate within each phase. In addition, the natural beat-to-beat variation caused for example by respiration, movement, and noise can also be seen. Overall, the signals measured with the bandages and the regular electrodes have very similar beat-to-beat variability patterns. Nevertheless, electromyographic noise during the walking phase in the regular electrode measurements seems to have been more abundant in this case (middlemost signals on the right), and the bandage signals seem to include a bit lower frequency variation during running (lowest signals on the left).
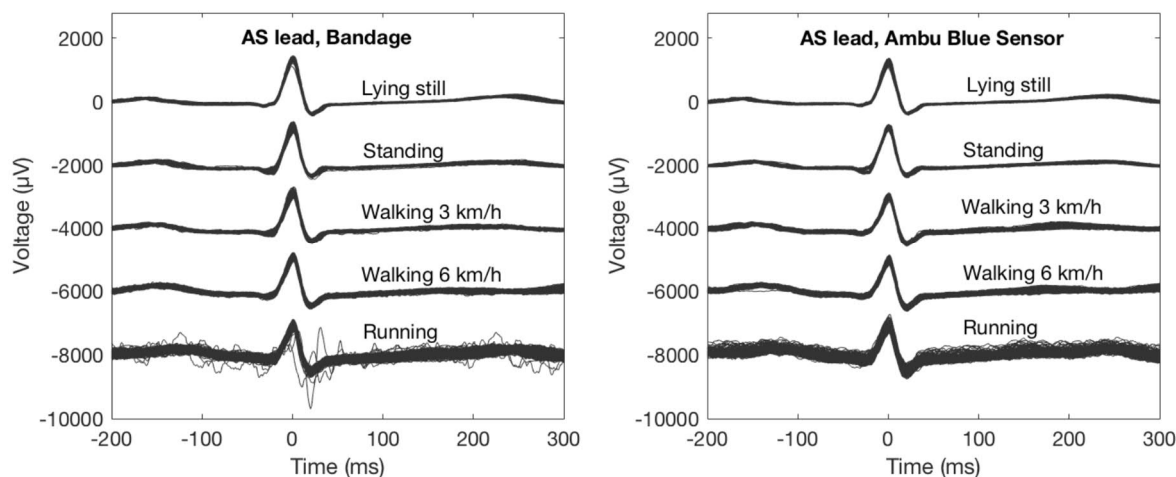
Figure 3. Superimposed beats in AS lead measured with the bandage (left) and ordinary electrodes (right) during lying still, standing, walking (3 km/h), brisk walking (6 km/h), and running (10 km/h). Each incremental activity level is biased by -2 mV from top to bottom to show the expected increasing beat-to-beat variability of the signals. (Volunteer number 24)

In addition to the similar beat-to-beat variation, the mean shape of the signals measured with the bandage and the regular electrodes look similar. This is more clearly depicted in *Figure 4*, that shows the average heartbeat waveform in each of the leads and test phases for the same subject. The remaining levels of discrepancy e.g. at the R peak amplitudes are explained mostly by minute differences in electrode positioning, heart rate, respiration and movements between the two measurements.
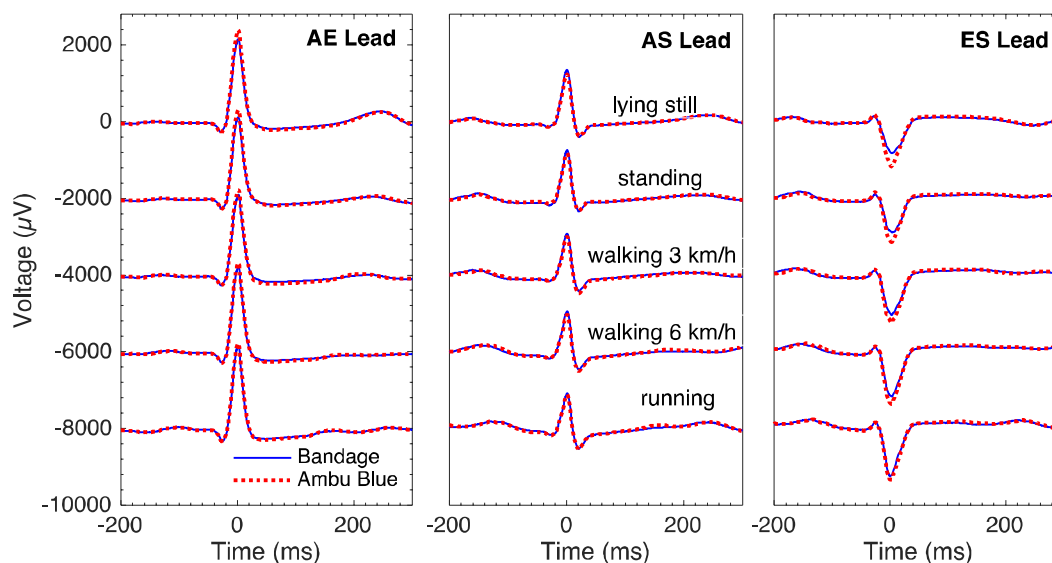
Figure 4. *Mean beats in AE, AS, and ES leads measured with the bandage (solid line) and ordinary electrodes (dotted line) during lying still, standing, walking (3 km/h), brisk walking (6 km/h), and running (10 km/h). Each incremental activity level is biased by -2 mV from top to bottom. (Volunteer number 24)*

In the previous figures, we have shown examples of data of one subject. To better summarize the beat-to-beat variability of the signals of all the subjects, we calculated how much variation there is with respect to the average shape of the QRS complex. More precisely, we subtracted the mean beats (***Figure 4***) from the individual beats (Figure 3, Figure S 2 and Figure S 3), and calculated the amount of the residual variation using the root-mean-square formula within a fixed time windows of 50 ms around the R-peak. ***Figure 5*** shows the boxplot of the deviations in the AS lead. Deviations in AE, and ES are shown in ***Figure S 4*** and ***Figure S 5*** in supporting information, respectively. Again, the results of the bandage measurements are illustrated on the left, and the ones obtained with regular electrodes on the right; and the measurement phases group the data from top to bottom in increasing work load order. The distribution of the beat-to-beat deviations of each subject is presented with a box with whiskers. Within each box, the horizontal line mark indicates the median, and the bottom and

top edges of the box indicate the lower and upper quartiles, respectively. The whiskers show

the smallest and largest deviations.
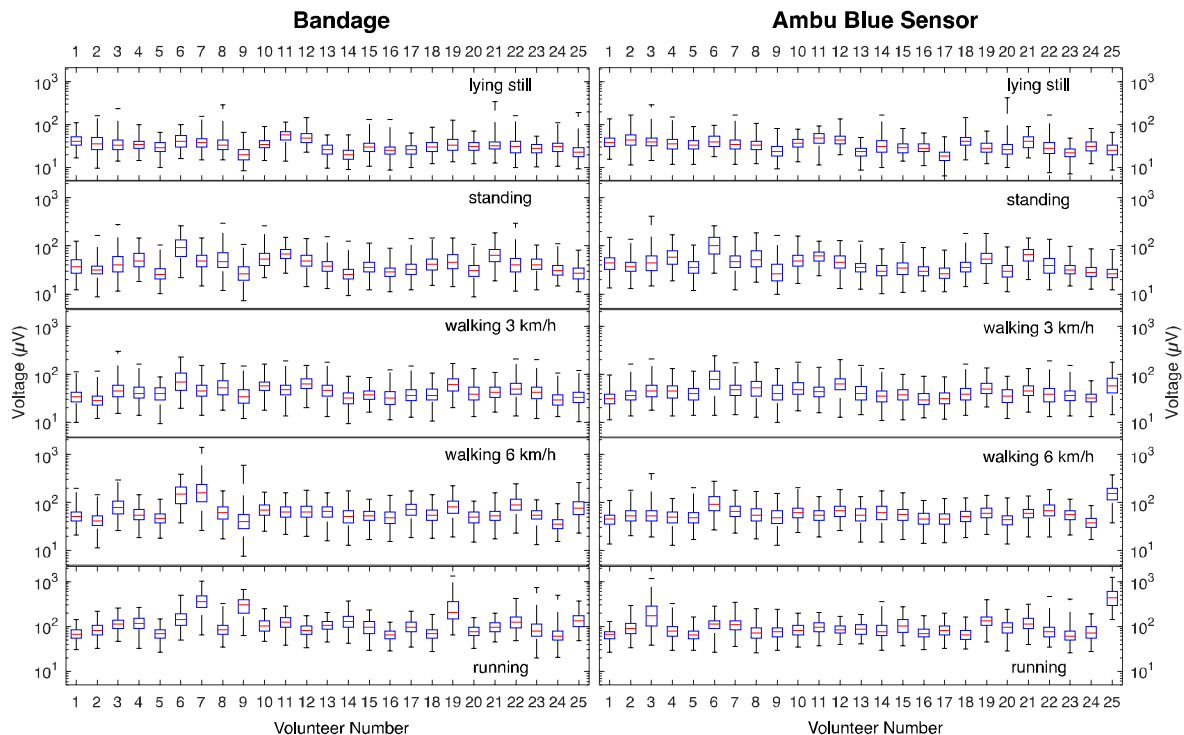
Figure 5. *RMS [µV] beat-to-beat variability of the QRS complex in the AS lead compared to the mean complex with the bandage (left) and ordinary electrodes (right) during lying stil, standing, walking (3 km/h), brisk walking (6 km/), and running (10 km/h) in all the subjects. The QRS complexes are selected with a fixed ±50 ms window around the R-peak.*

Generally, the deviations between the two measurements (left vs. right) are similar, but the

distribution is highly dependent on the subject. Especially, the median RMS-deviations of the

bandage and regular electrode measurements seem very similar, the mean absolute difference

between them being 16.5 µV, 22.3 µV, and 29.3 µV, in the leads AS, AE, and ES,

respectively, averaged across all the phases. This is further summarized in ***Figure 6*** that

collects the median discrepancies of each subject. There are some cases in which subject's

median beat-to-beat deviations in a certain exercise phase differ between the bandage and the

electrodes, which is seen as a departure from the diagonal line. Although overall these

deviations seem to be rather small and occur randomly in favor of the bandage or the regular electrodes for example due to some electromyographic artifact occurring in one test but not the other one, there is a slight tendency for this to happen mostly in the running phase with notably larger median deviations for the bandage for about half of the subjects. Mostly, this is explained by the somewhat larger low frequency baseline wander of the bandage signals during intensive exercise such as running, similar to what was seen in Figure 3, Figure S 2 and Figure S 3 (left bottom).
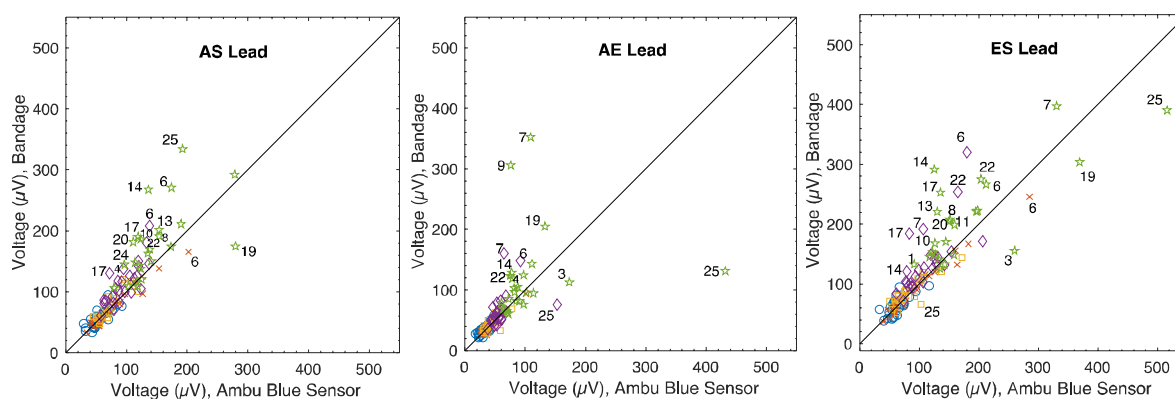
Figure 6. *Scatter plot comparison of median RMS [µV] beat-to-beat variabilities of the QRS waves in electrodes and bandages in all three channels AS, AE, and ES during lying still (circle o), standing (cross x), walking 3 km/h (square □), brisk walking 6 km/h (diamond ◊), and running 10 km/h (star ✩). Subject numbers for median RMS-deviations of over 35 µV are annotated*

Table 2 lists the corresponding Pearson correlation coefficients (*r*) of the median variabilities shown in Figure 6 to further quantify the aforementioned behavior. The correlation is strong when lying still, and very strong when standing, in all the leads. During normal and brisk walking, the correlation is strong in the AS and ES leads, but only moderate in the AE lead. The correlation is lowest being moderate in the AS and ES leads, and weak in the AE lead during running. Overall, the correlation in the AS and ES leads is strong and moderate in the AE lead, across all the phases. Stronger correlation arises from clear inter-individual

differences in the beat-to-beat variability that are similarly represented in the intra-individual electrode and bandage measurements. Despite the overall slight tendency of decreasing correlation with increasing level of activity, the correlation is most notably weakened due to the few distinct outlier cases especially in the AS lead during running and partly brisk walking.

Table 2. Correlations of the median RMS beat-to-beat variabilities of QRS waves between the electrode and bandage leads.

Phase	AS lead	AE lead	ES lead
Lying still	0.78	0.76	0.78
Standing	0.97	0.95	0.99
Walking	0.90	0.76	0.88
Brisk walking	0.79	0.41	0.71
Running	0.52	0.13	0.41
All combined	0.74	0.52	0.67

Finally, we also considered the amount of discrepancy of the mean beats (*Figure 4*) of all the subjects in clinical terms by extracting a portion of the ST-segment, and measuring the RMS-error between the mean bandage and the mean regular electrode beat in each of the leads. For the purposes of this study, the relevant ST-segment portion was defined to be the interval from 60 ms to 100 ms following the magnitude signal R peak to capture relevant differences.

Figure 7 shows the RMS-differences of the ST-segment portions of the mean beats. Current clinical guidelines for traditional 8/12-lead ECG (at rest) consider new ST-elevations or depressions at the J point in at least two contiguous leads larger than 100 µV - 200 µV – the exact threshold depending on the leads considered and subject's gender – to signify an ST-elevation myocardial infarction. [30] In most cases, the observed differences in *Figure 7* are

well below 50 µV with some notable exceptions. In the case of subject 22, for instance, the heart rate during the regular electrode measurements has been higher throughout most of the exercise protocol causing changes in the observed mean shape morphology. In this case, the recovery period between the tests may have not been long enough. The same is true for subject 15 but in this case, there has also been sizeable low frequency noise in the bandage signal starting already at the walking speed instead of the tendency of it to occur at a higher exercise intensity. For subject 25, the traditional electrode in S location exhibits movement artifact and contact issues during running phase which affects both AS and ES leads. Similar issue is encountered with subject 9 in which case the bandage E electrode shows contact problems. It is also worth noting that in cases such as subjects 6, 9, 16, 17, and 19 somewhat high ST-level differences are observed during the rest phase lying supine but the discrepancy is diminishing with the increasing intensity.
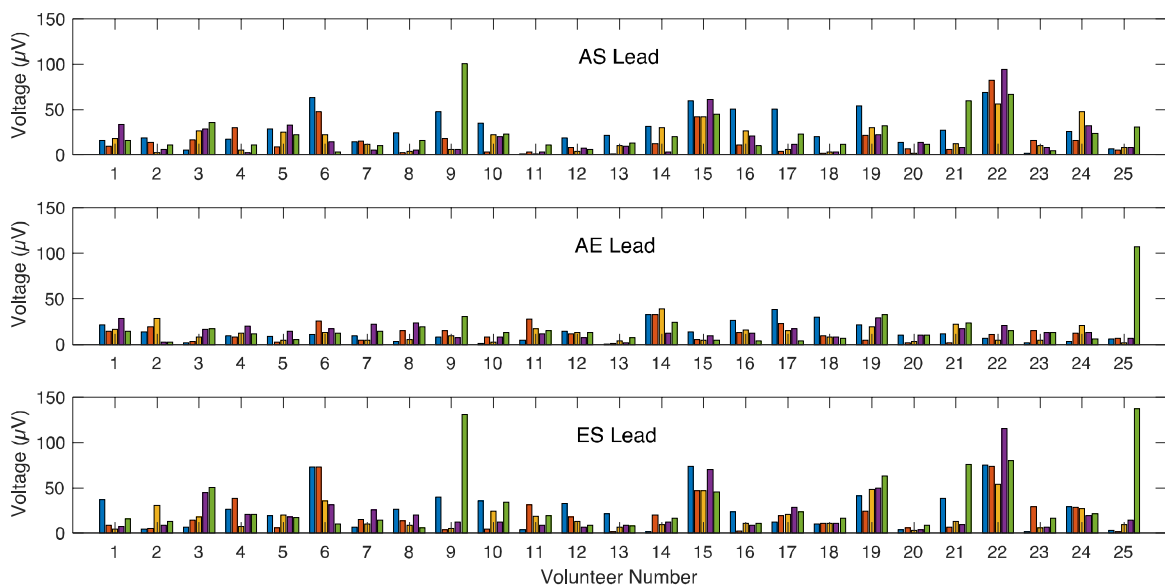
Figure 7. RMS differences in ST-segments of the mean beats between bandage and electrodes signals in all three channels AS (top), AE (middle), and ES (bottom). For each of the 25 subjects, the grouped bars show the RMS-difference during lying still, standing, walking (3 km/h), brisk walking (6 km/h), and running (10 km/h) from left to right.

3. Conclusion

Interindividual variation in e.g. electromyographic noise levels and the amount of movement artifacts were large in both measurement modalities during exercise. However, the overall signal quality is similar with the proposed bandage compared to the traditional electrodes in both average behavior as well as in beat-to-beat variation of the signals intra-individually throughout the exercise modalities. Differences between the mean beat ST-levels between the regular electrodes and the bandage were small for most subjects, but a few showed differences during supine rest which diminished towards increasing exercise intensity. This could be related to the characteristics of the persons, such as their anatomy and exact body position during lying pose, as well as physiological status such as cold or warm skin and amount of perspiration.

The bandage seems to be slightly more susceptible to the development of low frequency noise with a frequency related to the cadence and a power related to the exercise intensity. The noise is likely caused by upper torso soft tissue motion due to heel strike impacts, upper limb movements and torso rotations, as the bandage system ties skin tissues on the upper torso together more rigidly than individual electrodes. More comprehensive explanation is presented in the supporting information (*Figure S 6 -Figure S 9*). Bandage - measurement device interface and the shape of the bandage should be carefully designed to accommodate certain physiological characteristics such as persons with large breasts. More elastic and stretchable construction between the electrode sites could make the whole bandage system less rigid on the skin lessening susceptibility to movement related low frequency interference and disturbance.

4. Experimental Section

Printed electrodes fabrication: The outline of the fabrication process for the printed bandage is presented in the.[31] Printed electrodes and the circuitry are screen printed using TIC SCF-300 screen printer and CI-4040 stretchable Ag/AgCl ink (ECM, USA). The ink contains 40 – 50 wt% silver powder and 5 – 15 wt% silver chloride powder diluted in a diethylene glycol ethyl ether acetate solvent. Printing is done on a 50-µm-thick Platilon 4201 AU thermoplastic polymer substrate (Covestro, Germany). Tensile strain at break is 550% and tensile stress at 50% strain is 5-7 MPa and at break 550 MPa for this polyurethane film according to the manufacturer. After printing, the printed pattern is annealed in a convection oven at 130 °C for 30 minutes.

The print, with the polyurethane substrate, is heat laminated with Opsite Flexifix which is a transparent polyurethane film with an acrylic adhesive layer. The adhesive layer is used to attach the bandage to the skin. One additional 50-µm-thick polyurethane layer is laminated on top of the bandage material and print layers. Round shape pieces of 0.89-mm-thick AG635 sensing gel (Axelgaard Manufacturing CO., Ltd., USA) were used at the electrode-skin interface to form a stable electrical contact. This hydrogel material is designed and formulated specifically for electrocardiogram and electromyogram monitoring applications and according to our measurements the impedance of the bandage is at the acceptable level for ECG measurements.

Signal quality testing protocol: Chest hair was shaved prior to the recordings underneath the bandage location area. Next the skin was wiped with Desinfectol H (Berner Oy, Finland) disinfectant and dead skin cells were scraped off with Red Dot prep tape (3M). The bandage was then fixed in place and Faros 360 data recording device, configured in unipolar

measurement mode, was attached to the bandage with a micro-USB connector. Micro-USB connector contained 100 kΩ series resistors used for high voltage protection. Flexifix adhesive film was used to secure Faros in place and to minimize any mechanical stress to the micro-USB connector. Faros 360 was turned on and the participant was asked to perform the physical activities presented the following activities: Lying still in supine position (5 min), standing (5 min), walking 3 km/h (5 min), walking 6 km/h (5 min), running 10 km/h (2 min) and sitting (5 min). After activities the data collection device was switched off, bandage was removed and the participant had a one-hour rest.

Commercially available Ambu Blue Sensor R-00-S sensors were placed on participants' skin in the beginning of the second measurement using the same electrode locations as with the printed electrode bandage. The data collection device was turned on and the participant performed the previously mentioned physical activities. The data collection device was then switched off, the electrodes were removed and the test ended. The test arrangement was randomized so that the volunteers started the tests randomly either with the bandage or the Ambu Blue sensors.

ECG signals were measured at the sampling rate of 1000 Hz. As a preprocessing step before further analysis, baseline wandering was reduced by applying a digital 12th order Butterworth filter having 0.67 Hz cut-off frequency in both the forward and reverse directions using the zero-phase method in accordance with clinical guidelines.[32,33] QRS complexes were detected using a simple multilead R peak detector that operated on the magnitude signal of the a band-pass filtered AS and AE leads, i.e. on

17

$$u_{MAG} = \sqrt{u_{AS}^2 + u_{AE}^2} \qquad\qquad (1)$$

where u_{AS} and u_{AE} are the band-pass filtered (1–40 Hz) lead signals. In the magnitude signal, the R-peaks were detected as local maxima agreeing to fixed constraints on peak amplitudes and interpeak distances (amplitude 1.3 mV & 1 mV higher with respect to neighboring peaks; RR interval larger than 270 ms). Results of the QRS-detection were also manually validated. Ectopic beats such as premature ventricular contractions (PVCs) were rejected based on abnormal width of the QRS complex. A beat was considered ectopic if it was 20 % wider than the median width of all the complexes at half QRS height. Beats containing sudden level changes e.g. due to connector movement were rejected as artifacts (> 1 mV/sample). For each exercise test protocol phase, the cardiac cycles were grouped together within the same phase based on the protocol time table leaving ten second ambiguity/transition regions around the phase changes in both directions. All the non-rejected cycles considered normal were extracted using a fixed window from -200 ms to 300 ms around the detected magnitude signal R-peak. Finally, it should be noted that the band-pass filtering step was only used for the QRS and ectopic beat detection, and all further analysis is based on the baseline wander reduced signal.

Ethical statement This study was accepted by the Ethics Committee of the Tampere Region. All volunteer test subjects were informed on the purpose of the study and informed signed consents were obtained from them.

Supporting Information

Supporting Information is available from the Wiley Online Library or from the author.

Received: ((will be filled in by the editorial staff))

Revised: ((will be filled in by the editorial staff))

Published online: ((will be filled in by the editorial staff))

References

[1]   WHO, "Cardiovascular diseases (CVDs)," can be found under

https://www.who.int/news-room/fact-sheets/detail/cardiovascular-diseases-(cvds),

2017.

[2]   S. R. Steinhubl, E. D. Muse, E. J. Topol, *Sci. Transl. Med.* **2015**, *7*, 283rv3.

[3]   J. P. DiMarco, J. T. Philbrick, *Ann. Intern. Med.* **1990**, *113*, 53.

[4]   F. Ershad, K. Sim, A. Thukral, Y. S. Zhang, C. Yu, *APL Mater.* **2019**, *7*, DOI

10.1063/1.5060270.

[5]   A. K. Yetisen, J. L. Martinez-Hurtado, B. Ünal, A. Khademhosseini, H. Butt, *Adv.

Mater.* **2018**, *30*, DOI 10.1002/adma.201706910.

[6]   E. Fung, M.-R. Järvelin, R. N. Doshi, J. S. Shinbane, S. K. Carlson, L. P. Grazette, P.

M. Chang, R. S. Sangha, H. V. Huikuri, N. S. Peters, *Front. Physiol.* **2015**, *6*, DOI

10.3389/fphys.2015.00149.

[7]   L. Y. Chen, N. S. Roetker, A. R. Folsom, A. Alonso, H. S. R, *Circulation* **2015**, *132*,

A11721.

[8]   D.-H. Kim, N. Lu, R. Ma, Y.-S. Kim, R.-H. Kim, S. Wang, J. Wu, S. M. Won, H. Tao, A. Islam, Yu, K. J., Kim, T.-i., R. Chowdhury, M. Ying, L. Xu, M. Li, H. -J. Chung, H. Keum, M. McCormick, P. Liu, Y.-W. Zhang, F. G. Omenetto, Y. Huang, T. Coleman, J. A. Rogers, *Science (80-.).* **2011**, *333*, 838 LP.

[9]   J.-W. Jeong, W.-H. Yeo, A. Akhtar, J. J. S. Norton, Y.-J. Kwack, S. Li, S.-Y. Jung, Y. Su, W. Lee, J. Xia, Cheng, Huanyu, Y. Huang, W.-S. Choi, T. Bretl, J. A. Rogers, *Adv. Mater.* **2013**, *25*, 6839.

[10]   S. P. Lee, G. Ha, D. E. Wright, Y. Ma, E. Sen-Gupta, N. R. Haubrich, P. C. Branche, W. Li, G. L. Huppert, M. Johnson, H. B. Mutlu, K. Li, N. Sheth, J. A. Wright, Y. Huang, M. Mansour, J. A. Rogers, R. Ghaffari, *npj Digit. Med.* **2018**, *1*, 2.

[11]   E. Bihar, T. Roberts, Y. Zhang, E. Ismailova, T. Hervé, G. G. Malliaras, J. B. De Graaf, S. Inal, M. Saadaoui, *Flex. Print. Electron.* **2018**, *3*, DOI 10.1088/2058-8585/aadb56.

[12]   S. Nie, C. Zhang, J. Song, *Sci. Rep.* **2018**, *8*, DOI 10.1038/s41598-018-32152-4.

[13]   S. R. Krishnan, C.-J. Su, Z. Xie, M. Patel, S. R. Madhvapathy, Y. Xu, J. Freudman, B. Ng, S. Y. Heo, H. Wang, T.R. Ray, J. Leshock, I. Stankiewicz, X. Feng, Y. Huang, P. Gutruf, J. A. Rogers, *Small* **2018**, *14*, DOI 10.1002/smll.201803192.

[14]   J. Kim, J. R. Sempionatto, S. Imani, M. C. Hartel, A. Barfidokht, G. Tang, A. S. Campbell, P. P. Mercier, J. Wang, *Adv. Sci.* **2018**, *5*, 1800880.

[15]   S. R. Madhvapathy, Y. Ma, M. Patel, S. Krishnan, C. Wei, Y. Li, S. Xu, X. Feng, Y. Huang, J. A. Rogers, *Adv. Funct. Mater.* **2018**, *28*, DOI 10.1002/adfm.201802083.

[16]   J. Sun, Y. Zhao, Z. Yang, J. Shen, E. Cabrera, M. J. Lertola, W. Yang, D. Zhang, A. Benatar, J. M. Castro, D. Wu, L. J. Lee, *Nanotechnology* **2018**, *29*, DOI 10.1088/1361-6528/aacc59.

[17]   J. Kim, I. Jeerapan, S. Imani, T. N. Cho, A. Bandodkar, S. Cinti, P. P. Mercier, J. Wang, *ACS Sensors* **2016**, *1*, 1011.

[18]   R. A. Nawrocki, H. Jin, S. Lee, T. Yokota, M. Sekino, T. Someya, *Adv. Funct. Mater.* **2018**, *28*, DOI 10.1002/adfm.201803279.

[19]   W. Dong, X. Cheng, T. Xiong, X. Wang, *Biomed. Microdevices* **2019**, *21*, 6.

[20]   Y. Yamamoto, D. Yamamoto, M. Takada, H. Naito, T. Arie, S. Akita, K. Takei, *Adv. Healthc. Mater.* **2017**, *6*, DOI 10.1002/adhm.201700495.

[21]   M. Mosallaei, J. Jokinen, M. Honkanen, P. Iso-Ketola, M. Vippola, J. Vanhala, M. Kanerva, M. Mäntysalo, *IEEE Trans. Components, Packag. Manuf. Technol.* **2018**, *8*, 1344.

[22]   Z. G. Yan, B. L. Wang, K. F. Wang, *Compos. Part B Eng.* **2019**, *166*, 65.

[23]   L. Ren, S. Xu, J. Gao, Z. Lin, Z. Chen, B. Liu, L. Liang, L. Jiang, *Sensors* **2018**, *18*, DOI 10.3390/s18041191.

[24]   M. Chi, J. Zhao, Y. Dong, X. Wang, *Mater.* **2019**, *12*, DOI 10.3390/ma12060971.

[25]   W. Liu, W. Zhou, S. Liu, C. Zhang, S. Huang, Y. Li, K. S. Hui, *Sensors Actuators A Phys.* **2018**, *269*, 515.

[26]   G. Li, S. Wang, Y. Y. Duan, *Sensors Actuators B Chem.* **2018**, *277*, 250.

[27]   T. Takeshita, M. Yoshida, Y. Takei, A. Ouchi, A. Hinoki, H. Uchida, T. Kobayashi, *Sci. Rep.* **2019**, *9*, 5897.

[28]   M. Mantysalo, T. Vuorinen, V. Jeihani, A. Vehkaoja, in *Proc. SPIE - Int. Soc. Opt. Eng.*, **2017**.

[29]   V. Jeyhani, T. Vuorinen, K. Noponen, M. Mäntysalo, A. Vehkaoja, in *Kyriacou E., Christofides S., Pattichis C. XIV Mediterr. Conf. Med. Biol. Eng. Comput. 2016*, SPringer, Cham, **2016**, pp. 1144–1149.

[30] P. T. O'Gara, F. G. Kushner, D. D. Ascheim, D. E. Casey, M. K. Chung, J. A. de Lemos, S. M. Ettinger, J. C. Fang, F. M. Fesmire, B. A. Franklin, C. B. Granger, H. M. Krumholz, J. A. Linderbaum, D. A. Morrow, L. K. Newby, J. P. Ornato, O. Narith, M. J. Radford, J. E. Tamis-Holland, C. L. Tommaso, C. M. Tracy, Y. J. Woo, D. X. Zhao, *Circulation* **2013**, *127*, e362.

[31] T. Vuorinen, A. Vehkaoja, V. Jeyhani, K. Noponen, A. Onubeze, T. Kankkunen, A.-K. Puuronen, S. Nurmentaus, S. P. Preejith, J. Joseph, T. Seppanen, M. Sivaprakasam, M. Mantysalo, in *2016 6th Electron. Syst. Technol. Conf. ESTC 2016*, **2016**.

[32] A. V Oppenheim, R. W. Schafer, J. R. Buck, *Discrete-Time Signal Processing (2Nd Ed.)*, Prentice-Hall, Inc., Upper Saddle River, NJ, USA, **1999**.

[33] P. Kligfield, L. S. Gettes, J. J. Bailey, R. Childers, B. J. Deal, E. W. Hancock, G. van Herpen, J. A. Kors, P. Macfarlane, D. M. Mirvis, O. Pahlm, P. Rautaharju, G. S. Wagner, M. Josephson, J. W. Mason, P. Okin, B. Surawicz, H. Wellens, *Circulation* **2007**, *115*, 1306.

Supporting Information

**Printed, skin-mounted electrodes for ECG measurements**

Tiina Vuorinen*, Kai Noponen, Timo Onnia, Antti Vehkaoja, Eeva Laakso, Susanna Leppänen, Kirsi Mansikkamäki, Tapio Seppänen & Matti Mäntysalo

Figure S 1. is presenting how the measurement systems were worn during signal quality testing. In *Figure S 1* a) a volunteer is wearing the printed bandage and Faros 360 data collecting device and in *Figure S 1* b) the volunteer is wearing Ambu Blue sensors.
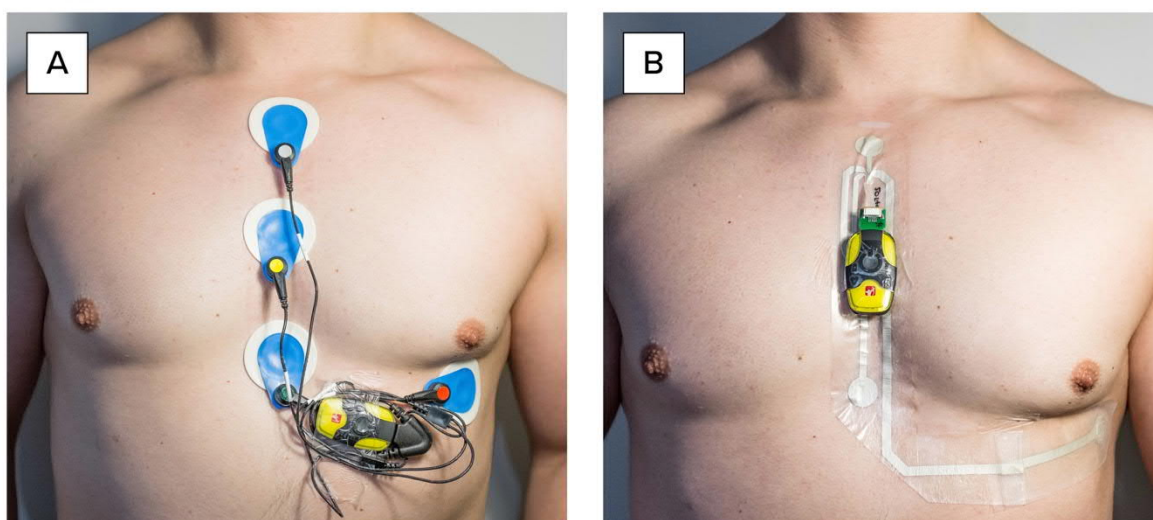

Figure S 1. A) Printed electrodes and Faros 360 device attached to the volunteer's chest. B) Ambu Blue sensors with Faros 360.

Figure S 2 and **Figure S 3** are presenting superimposed beats in AE and ES leads measured with the bandage (left) and ordinary electrodes (right) during lying still, standing, walking (3 km/h), brisk walking (6 km/h), and running (10 km/h).
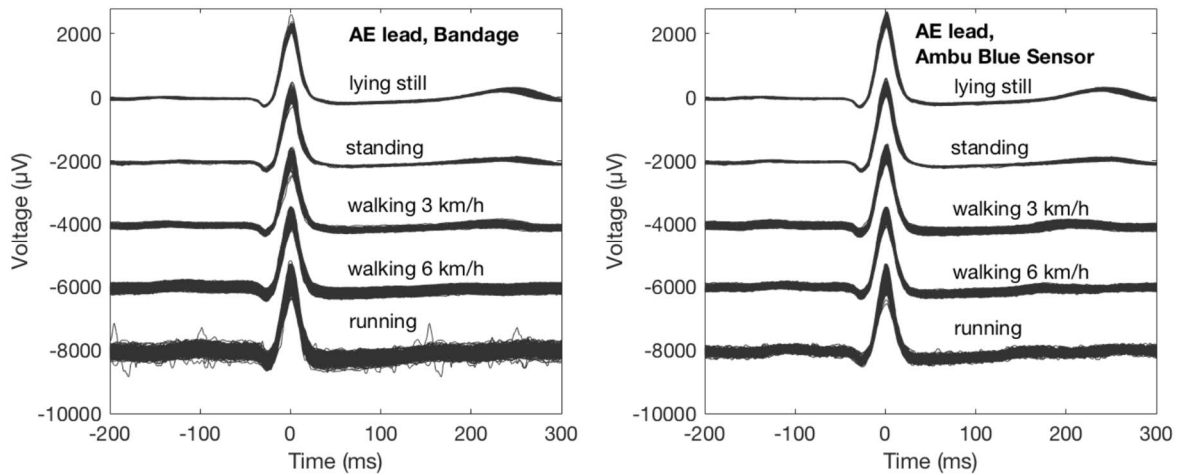
Figure S 2. *Superimposed beats in AE lead. Each incremental activity level is biased by -2 mV from top to bottom to show the expected increasing beat-to-beat variability of the signals. (Volunteer number 24)*
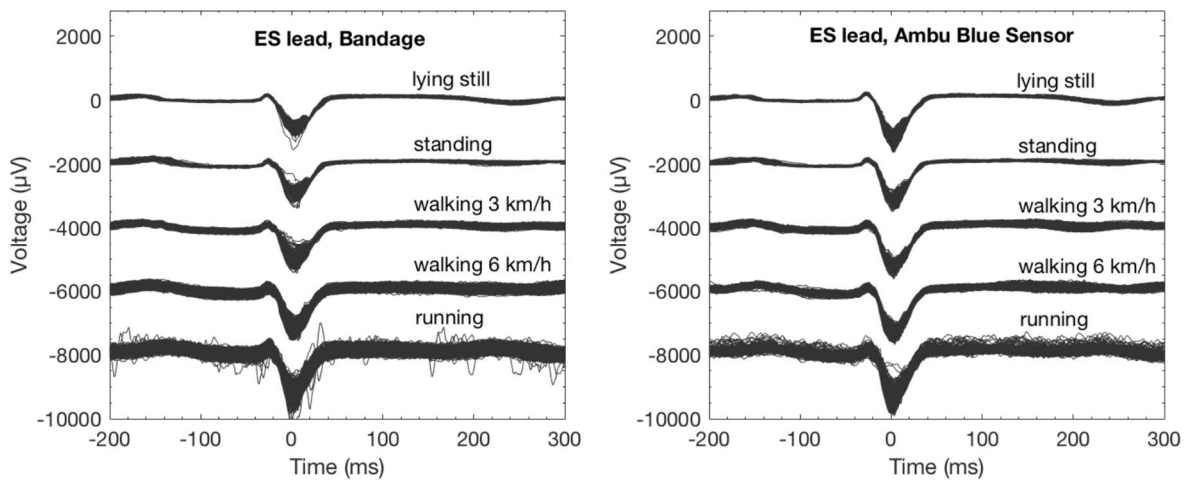

Figure S 3. *Superimposed beats in ES lead. Each incremental activity level is biased by -2 mV from top to bottom to show the expected increasing beat-to-beat variability of the signals. (Volunteer number 24)*

Figure S 4 and ***Figure S 5*** are showing RMS [μV] beat-to-beat variability of the QRS waves in the AE and ES leads compared to the mean complex with the bandage (left) and ordinary electrodes (right) during lying still, standing, walking (3 km/h), brisk walking (6 km/), and running (10 km/h) from top to bottom in all the subjects.
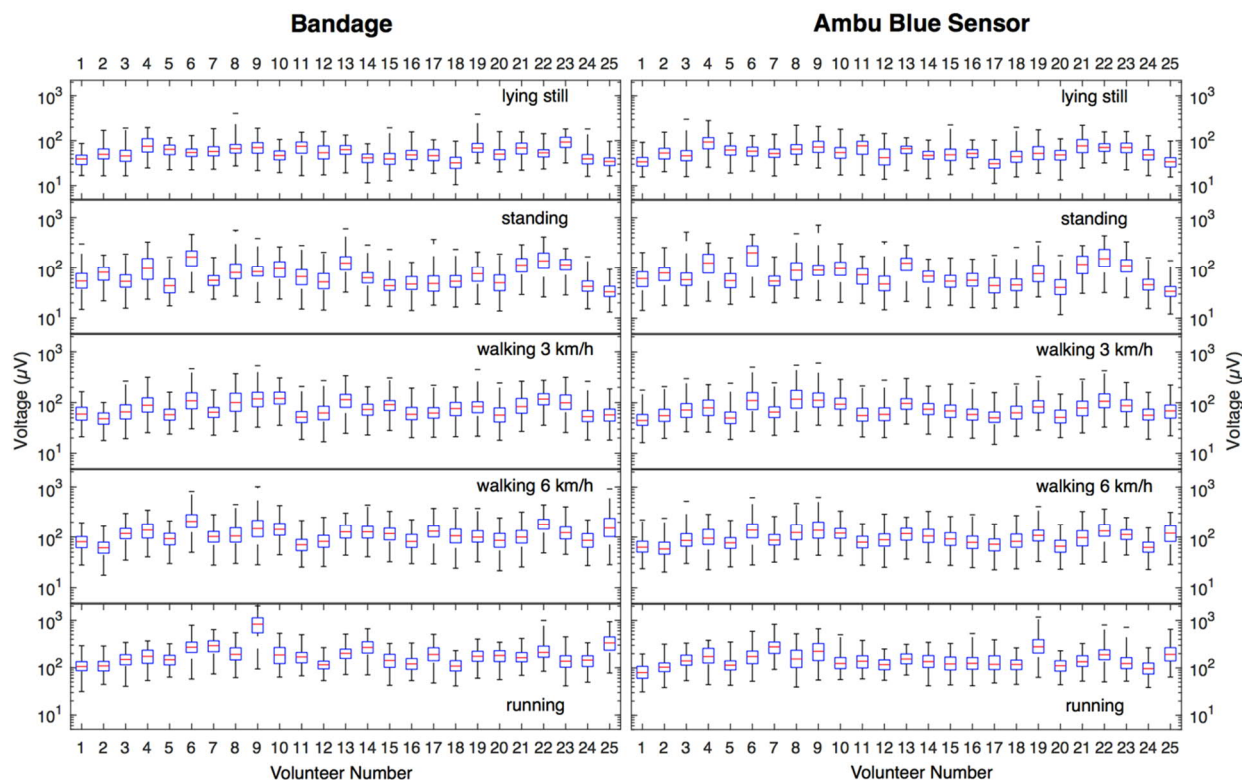
Figure S 4. RMS [µV] beat-to-beat variability of the QRS waves in the AE lead compared to the mean complex with the bandage (left) and ordinary electrodes (right). The QRS complexes are selected with a fixed ±50 ms window around the R-peak.
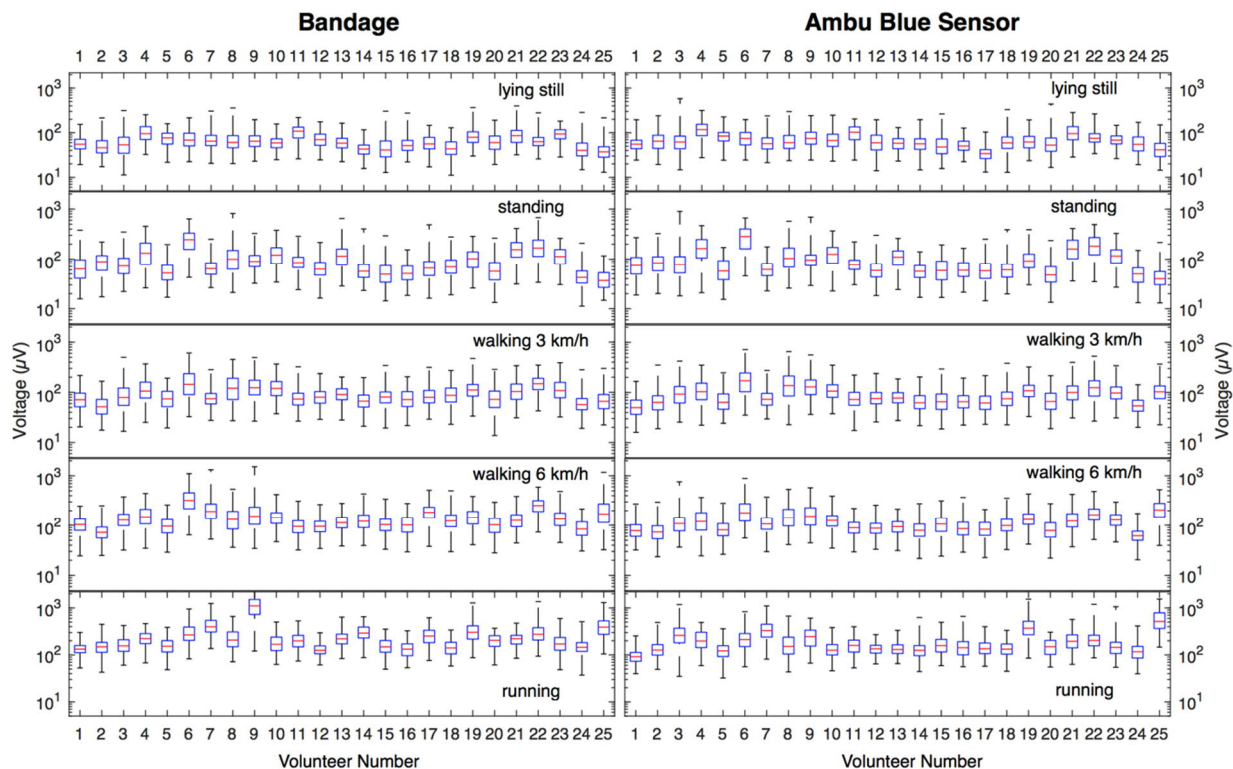
Figure S 5. RMS [µV] beat-to-beat variability of the QRS waves in the ES lead compared to the mean complex with the bandage (left) and ordinary electrodes (right). The QRS complexes are selected with a fixed ±50 ms window around the R-peak.

Figure S 6 - *Figure S 9* depict the spectrograms of the electrode and bandage measurements of the subjects 10 and 6. Starting from the top, the spectrograms of the three EAS lead ECGs (AE, AS & ES) are shown, followed by the spectrograms of the simultaneously measured three accelerometer channels X, Y and Z. The changes of the measurement phases have been indicated with vertical lines.
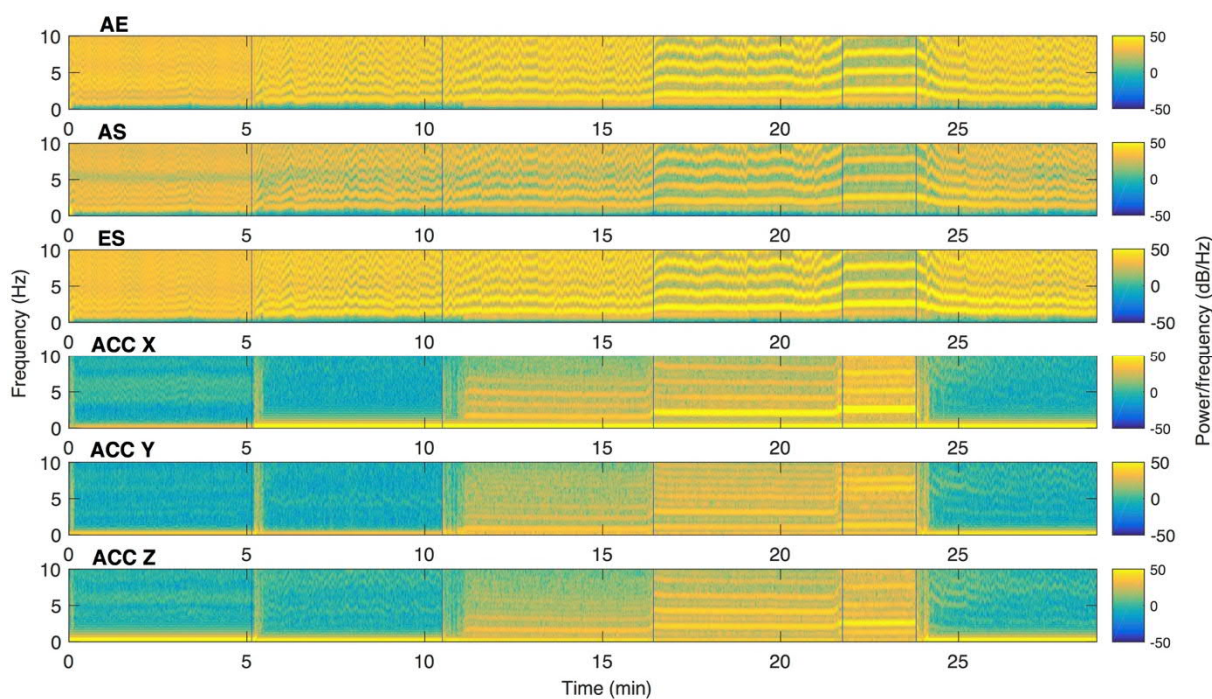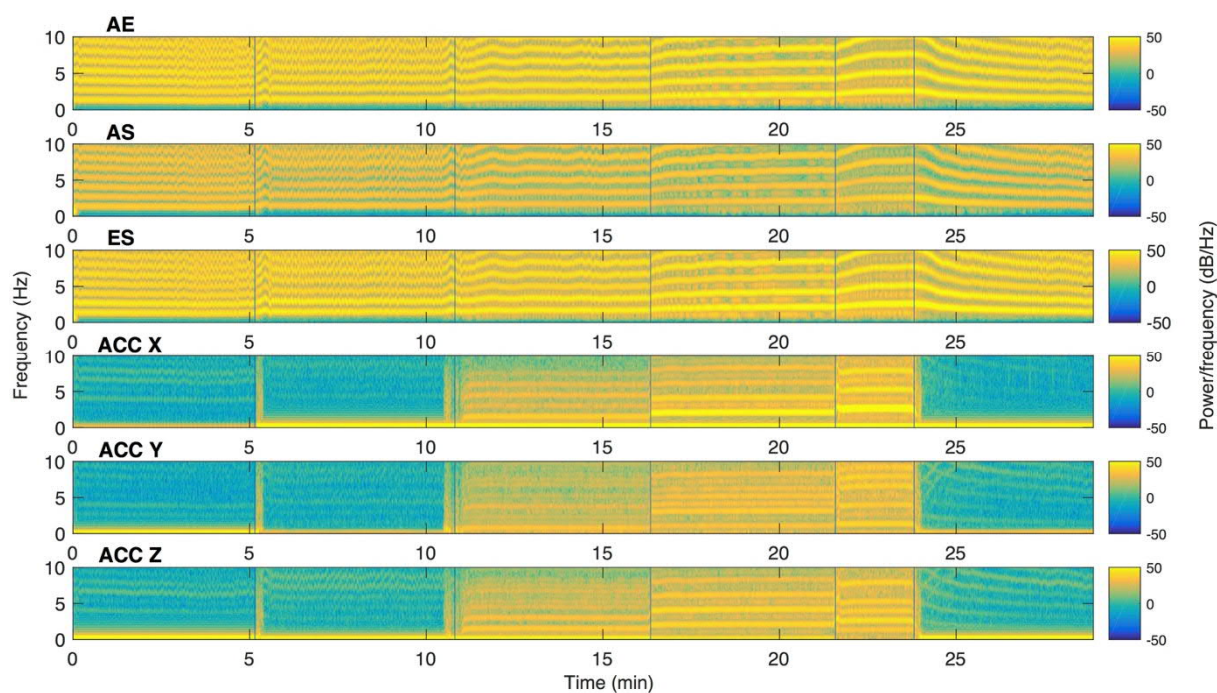

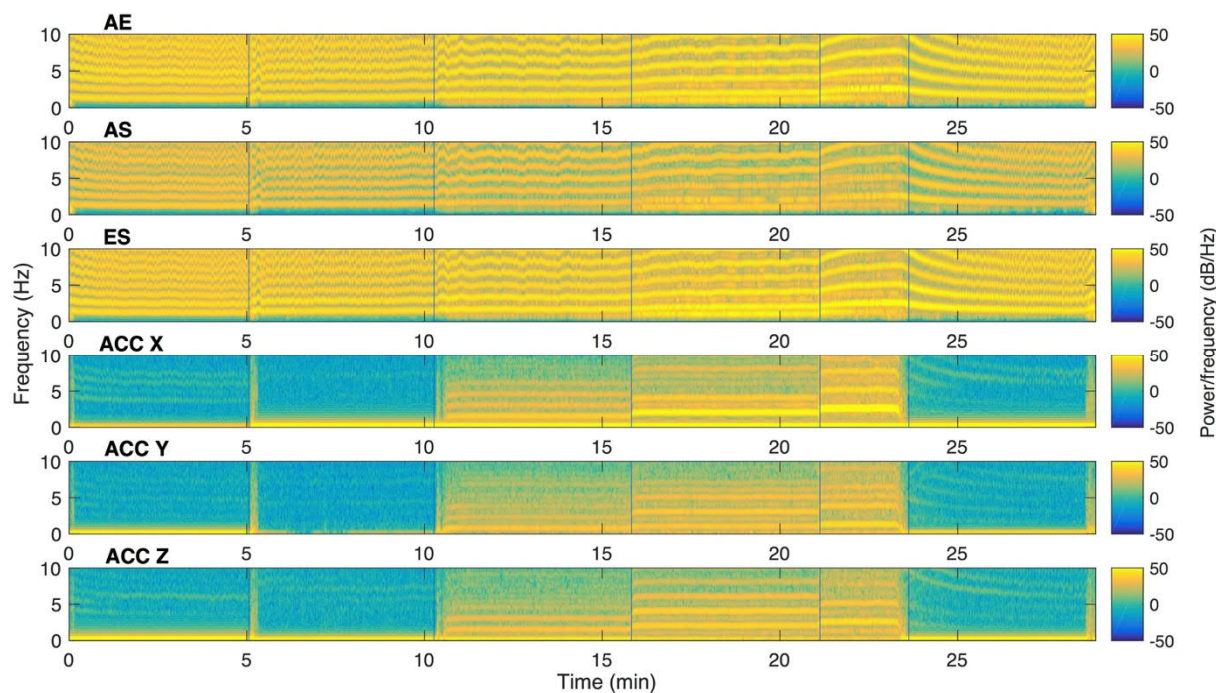*Figure S 6. ECG and accelerometer spectrograms from the electrode measurements. (volunteer number 10).*
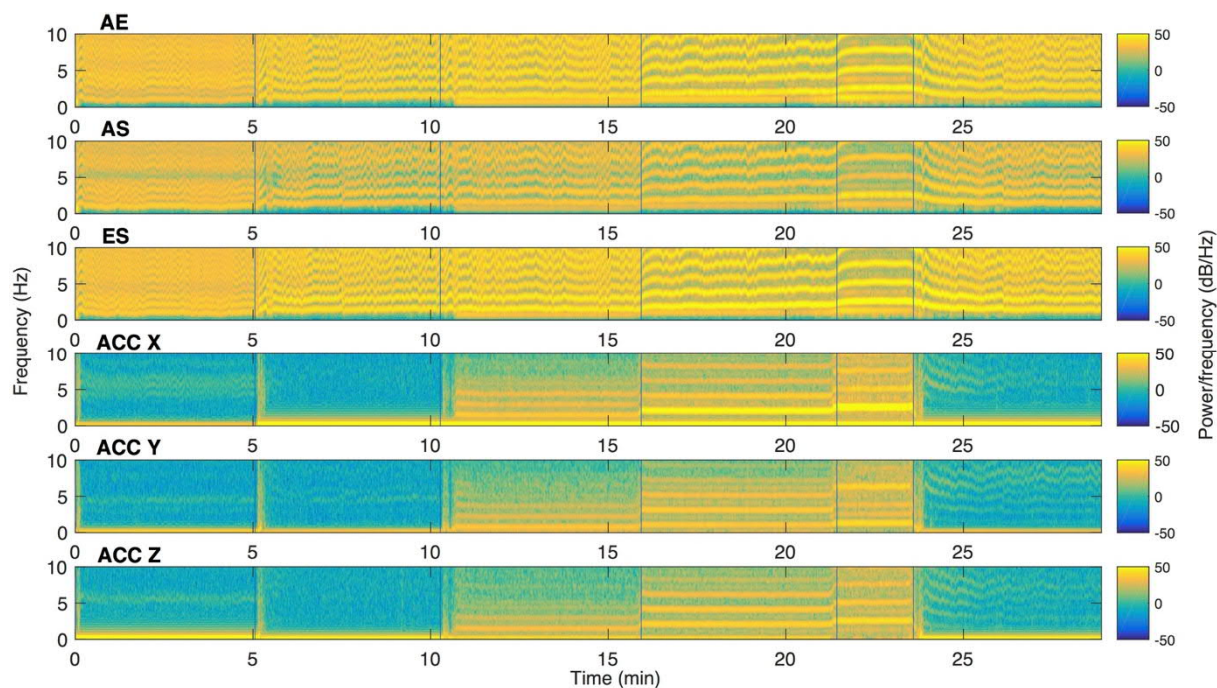
Figure S 7. ECG and acceleration spectrograms from the bandage measurements. (volunteer number 10).

Figure S 8. ECG and acceleration spectrograms from the electrode measurements. (volunteer number 6).

Figure S 9. *ECG and acceleration spectrograms from the bandage measurements. (volunteer number 6).*

The orientation of the measurement device is shown in ***Figure S 1***, and the internal accelerometer coordinate axes are as follows. The X axis is oriented towards the feet/ground, and thus the X channel measures mainly the vertical (longitudinal) movement. The Y axis is oriented to the anatomical left, and the Y channel represents mostly the frontal (mediolateral) movement. The Z axis is oriented towards the front of the subject, and the Z channel represents mainly the sagittal (anteroposterior) motion.

It can be seen from the figures that the onset of motion is accompanied with the onset of a low frequency ECG noise component in both the bandage and electrode measurements in all the EAS leads. The power of the noise component is correlated with the motion intensity (the accelerometer component power) in both the measurements, but it is higher in the bandage measurement than in the electrode measurement. Furthermore, this motion related noise

component disappears when the motion ceases in the resting phase, and the spectra return similarly to the resting baseline in both the measurements. Moreover, the frequency of the motion related ECG noise component changes in close association with the accelerometer spectral component frequencies being around half of the primary vertical cadence related component frequency, and about the same as the main frontal movement component frequency.

First, the device orientation difference between the bandage and electrode measurement was corrected by applying a 3D-rotation to the electrode measurement acceleration data to map it to the coordinate system of the bandage measurement. Second, the 25 Hz accelerometer data was resampled to 1000 Hz to match that of the ECG with cubic splines. Finally, the spectrograms were computed using a 3 second Hanning window, and 2 second overlap over the whole measurement including the resting phase at the end.